ROYAL SOCIETY OF CHEMISTRY

PAPER

Check for updates

Singlet oxygen formation from photoexcited P3HT:PCBM films applied in oxidation reactions†

Aleksandra Nyga, [ab] Agata Blacha-Grzechnik,*[ab] Przemysław Podsiadły,[b] Alicja Duda, [b] Kinga Kępska,[a] Maciej Krzywiecki, [c] Radosław Motyka, [b] René A. J. Janssen [d] and Przemysław Data [*a]

Poly(3-hexylthiophene) thin films containing carbon-based nanostructures, *i.e.* fullerenes such as buckminsterfullerene (C_{60}) or phenyl-C_{61}-butyric acid methyl ester (PCBM), or single-walled carbon nanotubes, were investigated as heterogeneous photosensitizers producing singlet oxygen ($^1O_2$) in aerated organic solvents. Thin films were deposited on borosilicate glass using spin coating and characterized by profilometry, UV-vis, Raman and XPS. Photogeneration of $^1O_2$ was confirmed by photooxidation of 1,3-diphenylisobenzofuran and by reaction of 1,5-dihydroxynaphthalene to juglone. The photochemical efficiency of the blends was found to depend on the carbon-based photosensitizer and can be increased by varying its concentration in the poly(3-hexylthiophene) matrix.

1. Introduction

Blends of conjugated polymers and carbon nanostructures, such as fullerenes and carbon nanotubes (CNTs), have been under high scientific interest for application in organic photovoltaic (OPV) devices[1–3] and have been extensively studied for their photophysical properties. In polymer:fullerene blends two competitive processes have been identified to occur from the initially-formed interfacial charge-transfer state: charge separation and charge recombination into a triplet state.[4] The efficiencies of these processes not only depend on the individual properties of the donor and acceptor in the blend, but also on their ratio and the layer morphology.[5,6] Triplet generation is considered as a significant drawback in OPV, because it reduces the short-circuit current density, open-circuit voltage, and power conversion efficiency, and in the presence of oxygen may lead to the formation of singlet oxygen ($^1O_2$) which is highly reactive and destructive for the photoactive layers.[7,8]

Though the formation of $^1O_2$ may be unfavorable for organic electronic devices, it received much scientific attention as an efficient oxidative agent in fine-chemicals synthesis, wastewater treatment, and in photodynamic therapy (PDT).[9–13] The direct optical excitation of triplet ground state oxygen to the singlet excited state is spin-forbidden, but $^1O_2$ formation is possible using photosensitizers. In such a process, a photosensitizer absorbs light, forming a singlet-excited state (S_1) and converts to a triplet-excited state (T_1) *via* intersystem crossing (ISC) that can subsequently transfer its energy in a spin-allowed reaction to ground state triplet oxygen ($^3O_2$) resulting in formation of singlet-state oxygen and the photosensitizer in the ground state.[9,13]

The most commonly studied photoactive molecules are organic dyes, transition metal complexes, and inorganic oxides.[9,10,13] In recent years, carbon-based photosensitizers have been shown to produce $^1O_2$ in good yields,[14] but practical applications are limited because these materials mainly absorb in the high-energy region. To circumvent this problem, additional organic chromophores can be introduced.[15–19] The high reactivity of $^1O_2$ causes its lifetime to be very short and it thus must be produced *in situ*, using either homogenous or heterogeneous photocatalysts. Immobilization of photosensitizers generally results in a decrease in their activity but may be beneficial for commercial applications.[10,20]

Reactive oxygen species (ROS), such as singlet oxygen, exhibit strong antimicrobial properties acting in a versatile way on bacteria, viruses, and fungi. The main advantage of photodynamic antimicrobial chemotherapy (PACT) is the absence of microbial resistance towards ROS, and that it does not cause the spread of drug-resistant bacteria.[19,21,22] High attention is put nowadays on the introduction of antimicrobial coatings in health-related areas to decrease the number of

[a] Centre for Organic and Nanohybrid Electronics, Silesian University of Technology, Konarskiego 22b, 44-100 Gliwice, Poland. E-mail: przemyslaw.data@polsl.pl, agata.blacha@polsl.pl

[b] Faculty of Chemistry, Silesian University of Technology, Strzody 9, 44-100 Gliwice, Poland

[c] Institute of Physics – CSE, Silesian University of Technology, Konarskiego 22b, 44-100 Gliwice, Poland

[d] Molecular Materials and Nanosystems & Institute for Complex Molecular Systems, Eindhoven University of Technology P.O. Box 513, 5600 MB, Eindhoven, The Netherlands

patients gaining nosocomial infections.[23] The introduction of photoactive antimicrobial coatings would allow also reduce the use of chlorinated, toxic disinfectants. Various approaches for the immobilization of photoactive molecules, mainly dyes, have been explored, *e.g.* the non-covalent immobilization in a polymer matrix, like cellulose acetate,[24] or covalent binding at a surface.[25] In the first case a high antimicrobial activity has been reported, however such materials may possess low stability, due to leaching of the photoactive molecule from the blend.[24,26] The covalent binding of dyes, *e.g.* Rose Bengal, to a polymer matrix, like polystyrene, polyamide, or poly(methyl methacrylate), can be achieved *via* chemical reaction between the matrix functional groups and the dyes.[27,28] The main disadvantage, however, is a more complicated multistep procedure.

In this study, we investigate the possibility of applying poly(3-hexylthiophene) (P3HT) layers containing carbon nanostructures, as a heterogeneous source of singlet oxygen. P3HT has been selected because it absorbs strongly in the visible region and its blends with carbon nanostructures can be easily deposited on solid supports. Moreover, their photophysical properties are well characterized in the literature. It has been shown that energy transfer from P3HT to fullerenes and carbon nanotubes occurs in solution[29,30] and in the solid-state,[31,32] and that such blends can produce singlet oxygen.[20] Here, P3HT is assumed to act both as support for the carbon-based photosensitizers and as a visible-light antenna. The blend layers were characterized with various spectroscopic techniques. Singlet oxygen photogeneration was investigated with 1,3-diphenylisobenzofuran (DPBF) in methanol under excitation with green light, which allowed for the determination of quantum yields of the photoprocess. On the other hand, oxidation of 1,5-dihydroxynaphthalene (DHN) to juglone in acetonitrile under white light illumination was demonstrated as an example of fine-chemical synthesis. The influence of the type of carbon photosensitizer and its content on the photoactive properties of the layer was studied.

2. Experimental

2.1. Materials

C60 (purity 99.9%) was purchased from Acros Organics. [6,6]-Phenyl-C_{61}-butyric acid methyl ester (PCBM) (purity 99.0%) and single-walled carbon nanotubes (SWCNTs) were obtained from Osilla Ltd. Regiorandom P3HT was synthesized following a well-established procedure (ESI†). Chlorobenzene ($>$99%, Acros Organics) was applied as a solvent for layer preparation. Sodium dodecyl sulfate ($>$98%, Sigma-Aldrich), isopropanol (99.5%), and acetone (95%) (both Acros Organics) were used for cleaning glass slides. 1,3-Diphenylisobenzofuran (DPBF, $>$97%) dissolved in methanol (99.9%, both Across Organic) was used as a singlet oxygen scavenger. The quantum yield of $^1O_2$ photogeneration was determined with Rose Bengal (Acros Organics) as a reference. Photooxidation under white light was tested with 1,5-dihydroxynaphthalene (DHN, 97%) in acetonitrile ($\geq$99.9% both from Sigma-Aldrich).

2.2. Photoactive layers deposition and characterization

P3HT layers containing carbon nanostructures as photosensitizers were formed on borosilicate glass slides (1 $\times$ 1 cm^2 or 3 $\times$ 3 cm^2, Präzisions Glas & Optik GmbH, PG&O) *via* spin coating (Laurell spin-coater, WS-650 M2-23). Before layer deposition, the glass substrates were cleaned with sodium dodecyl sulfate aqueous solution and then sonicated in acetone, pure water, and finally isopropanol. Carbon nanostructures and P3HT were dispersed in chlorobenzene in a 1 : 2 mass ratio, and additionally in 1 : 1 and 2 : 1 mass ratios in case of PCBM, and sonicated for 15 min. 30 mm^3 of the solution was dropped on the glass slide and spin coated for 30 s at a spinning rate of 2000 rpm.

A Veeco, Dektak 150 profilometer was used to determination the layer thickness, employing 1200 μm scanning length, a needle with a diameter of 12.5 μm, and a pressure force of 5.00 mg.

UV-vis spectra of the films were recorded with a HP 8452A spectrometer Raman spectra were recorded using Renishaw inVia Raman Microscope (Renishaw, Inc., New Mills, UK) equipped with a 514 nm diode laser, a 2400 line per mm grating, and a 50$\times$ objective. All spectra were smoothened and the baseline was subtracted utilizing Renishaw software.

X-ray photoelectron spectroscopy (XPS) analysis was done with PREVAC EA15 hemispherical electron energy analyzer with 2D multi-channel plate detector. Al-K_α X-ray source (PREVAC dual-anode XR-40B, 1486.6 eV) was used for sample irradiation. The measurements were conducted under 9 $\times$ 10^{-9} Pa base pressure. Pass energy was equal to 200 eV pass energy for survey spectra (scanning step 0.9 eV) and 100 eV (scanning step 0.05 eV) for high-resolution spectra acquisition. The binding energy scale was calibrated with respect to C–C component in the C1s region (284.8 eV).[33] The spectra were analyzed applying CASA XPS® software. Shirley function was used as a background and the product of Gaussian and Lorentzian functions were used for components fitting.

2.3. Singlet oxygen photogeneration

The effectiveness of the photoactive layers containing carbon-based nanomaterials in the process of singlet oxygen photogeneration was determined using a 0.06 mM solution of DPBF as specific $^1O_2$ quencher in methanol.[34,35] The reaction progress was monitored with a Hewlett Packard 8452A UV-vis spectrometer as the change in the DPBF absorbance at 410 nm. The process was conducted *in situ* in a standard 10 mm $\times$ 4 mm quartz cuvette (Hellma Analytics) under 532 nm laser irradiation (Oxxius, LCX-532L-150-CSB-PPA model having 150 mW maximum power reduced to 50 mW).[35] The quantum efficiency of the light-induced $^1O_2$ production was determined with the DPBF method and Rose Bengal as a standard having Φ_{RB} equal to 0.80 in CH_3OH.[36–39]

2.4. Material photooxidation of DHN

Selected P3HT-fullerene layers deposited on borosilicate glass slides were applied as a source of singlet oxygen in the

oxidation of DHN. *In situ* measurements were conducted in the set-up as for DPBF tests with a 100 W xenon lamp acting as a source of light. The initial concentration of DHN in acetonitrile was equal to 0.14 mM. The reaction with $^1O_2$ was followed by monitoring the decrease in the absorbance of DHN at 298 nm and the increase of the absorbance of the oxygen adduct, juglone, at 406 nm.

Photooxidation of DHN was also done in a 100 ml photoreactor. Nine glass slides (9 cm^2 each) covered with P3HT:PCBM were introduced into the photoreactor filled with a 0.0146 M solution of DHN in acetonitrile and illuminated with a xenon lamp. During the reaction, the mixture was magnetically stirred and bubbled with oxygen. After 4 h the reaction mixture was evaporated and the crude product was purified by column chromatography with dichloromethane as eluent. The structure of the product was confirmed by ^{1}H-NMR spectroscopy (Varian Unity Inova 300 MHz Spectrometer, CDCl$_3$).

3. Results and discussion

3.1. Deposition and characterization of photoactive layers

P3HT layers containing various carbon-based photosensitizers were deposited on glass substrates by spin coating. The spin-coating parameters were optimized, *i.e.* various rotation speeds were tested in the range between 500 and 4000 rpm, to obtain layers with *ca.* 35 nm thickness. The average thickness of the deposited layers is given in Table S1 (ESI†). Deposited layers were not subjected to heat treatment, *i.e.* thermal annealing, to minimize phase segregation and crystallization of fullerene and polymer,[40,41] that is known to assist charge separation between donor and acceptor units.[5,42–44]

Deposited layers were first characterized by UV-vis spectroscopy (Fig. 1). For P3HT a broad absorption band is observed between 400 and 600 nm with a maximum at *ca.* 510 nm attributed to its π–π* transition[42] and a shoulder at *ca.* 605 nm assigned to inter-chain stacking of P3HT and thus polymer ordering.[42,45,46] For fullerene-containing layers, the distinct fullerene absorption is visible at 340 nm and 334 nm for P3HT:C$_{60}$ and P3HT:PCBM, respectively.[47] The maximum of the P3HT π–π* absorption is blue-shifted to *ca.* 490 nm for P3HT:PCBM, and further to 455 nm for P3HT:C$_{60}$. Moreover, the significant decrease in the absorption of the shoulder at 605 nm is observed in the latter case suggesting less inter-chain interactions within P3HT upon addition of C$_{60}$.[48,49] On the other hand, the UV-vis spectrum of the P3HT:SWCNT film almost completely coincides with P3HT-only spectrum, indicating that at this concentration of SWCNTs the polymeric inter-chain interactions remain dominant over interactions of P3HT with SWCNTs.[31,48] The presence of carbon nanotubes in the blend is confirmed by weak absorption peak appearing close to 700 nm.[31]

The chemical composition of the layers was also analyzed with Raman spectroscopy (Fig. 2). For all spectra, characteristic bands of P3HT are observed. The deformation vibration of the C–S–C bond arises at *ca.* 720 cm^{-1}, the C–C skeletal stretching at 1379 cm^{-1}, while the C=C stretching vibrations occur at 1450 cm^{-1}.[43] The latter is broadened and slightly shifted to higher wavenumbers for fullerene-containing layers, which is due to the additional contribution of the "pentagonal pinch" A$_g$ mode vibrations of C$_{60}$ spheres[50] and may suggest the lower order and crystallinity of the P3HT.[51] Raman spectra of P3HT:SWCNT coating exhibit additional signal typically observed for CNTs, so-called G band at 1593 cm^{-1}.[2] However, in this case, the C=C stretching vibration band of thiophene ring, and thus order of polymeric matrix seems unaffected by the introduction of carbon nanotubes,[51] which is in agreement with above-mentioned UV-vis results.

A XPS survey spectrum recorded for the P3HT:PCBM film (Fig. S1a, ESI†) confirms full coverage of the glass substrate. Moreover, basing on survey spectra and C1s region (see Fig. S1c, ESI†), no signals of impurities coming from the solvent or reagents used for P3HT synthesis are observed. The position of S2p$_{3/2}$ component in S2p high-resolution spectrum
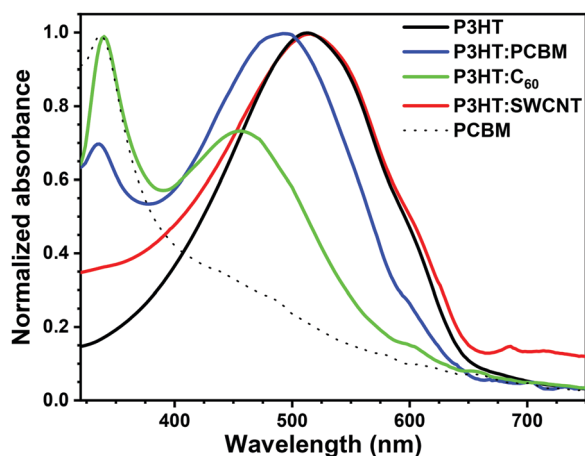

Fig. 1 UV-vis spectra of P3HT, P3HT:PCBM (2:1), P3HT:C$_{60}$ (2:1), P3HT:SWCNT (2:1) and PCBM layers deposited on borosilicate glass.
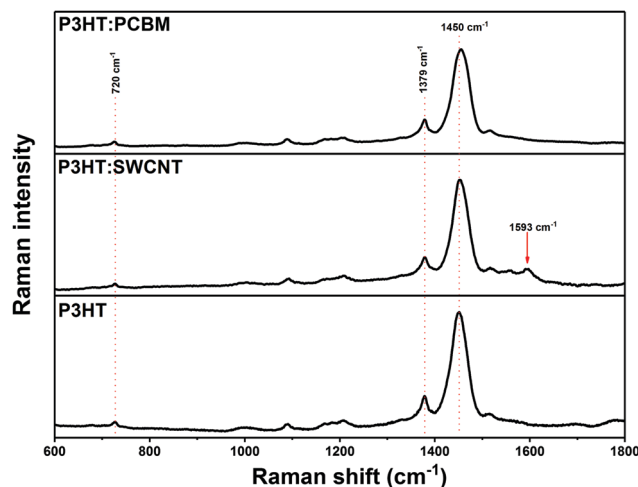

Fig. 2 Raman spectra of P3HT:PCBM (2:1), P3HT:SWCNT (2:1) and P3HT photoactive layers deposited on borosilicate glass.

(Fig. S1b, ESI†) suggests that polythiophene exists in its neutral form.[52,53]

3.2. Photogeneration of singlet oxygen

The photoactive layers were tested as a heterogeneous source of singlet oxygen in photooxidation reactions. As mentioned, P3HT plays a double role. First of all, it is used as a matrix for carbon-based photosensitizers and second, it may enhance absorption of visible light for $^1O_2$ production.

First, the process of singlet oxygen photogeneration was investigated with DPBF, which is a specific $^1O_2$ quencher.[34] The UV-vis spectra of a DPBF solution in methanol in contact with a P3HT:PCBM layer recorded during illumination with a green laser are shown in Fig. 3A. A clear decrease in the DPBF absorbance at 410 nm with time is observed, indicating that it is oxidized by singlet oxygen generated by irradiation of the P3HT:PCBM photoactive thin film.[17] This is further confirmed by control experiments, in which almost no drop in DPBF absorption is observed when the bare glass is illuminated or when the photoactive layer is in contact with the solution but not illuminated (Fig. 3B).

Fig. 3B shows the change of DPBF absorbance at 410 nm *vs.* time when various layers were illuminated. The largest drop in DPBF concentration after 25 min was observed for the P3HT layer containing PCBM. Under the applied conditions, P3HT itself exhibits poor photosensitizing properties.[20] Importantly, since no additional bands arise in the recorded UV-vis spectra in the course of the process (Fig. 3), the release of the fullerene into reaction mixture can be excluded. As shown in Fig. 4, the P3HT:PCBM photoactive layer retains its photoactivity towards singlet oxygen production in consecutive DPBF-tests, indicating that it can be effectively re-used. *Ca.* 10% decrease in the effectiveness of DPBF photooxidation was observed in the 7th run.

The quantum yield of singlet oxygen photogeneration (Φ) can be determined with respect to the well-known reference photosensitizers.[39,54] Here Rose Bengal was chosen. For
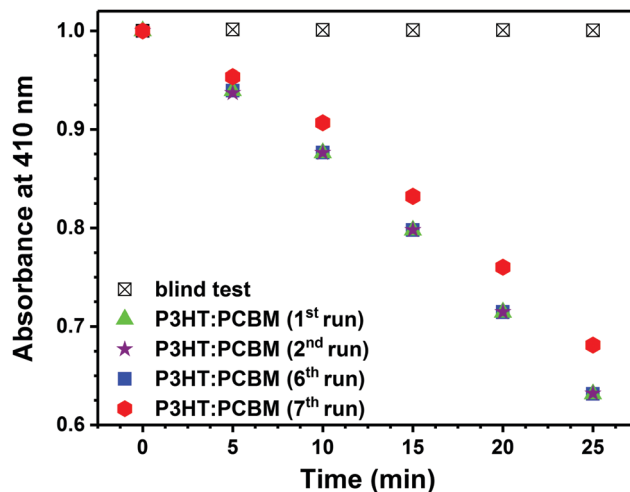
Fig. 4 The absorbance of DPBF at 410 nm as a function of time during consecutive illumination of P3HT : PCBM (2 : 1) deposited on borosilicate glass and bare borosilicate glass (blind test) with 532 nm laser.

P3HT:PCBM layers the quantum yield of singlet oxygen photogeneration was equal to 1.1% at a 2 : 1 mass ratio and increased to 4.2% at a 1 : 2 mass ratio (Table 1). Since the quantum yield of singlet oxygen photogeneration by the pristine PCBM layer (1.9%) is lower than that of P3HT : PCBM (1 : 2), energy transfer from P3HT to PCBM (which acts as the photosensitizer in the $^1O_2$ formation) is suggested.[17,31,32,55] We note that the energy of charge-separated state in P3HT:PCBM blends is at 1.14 eV and thus lower than the triplet energy of PCBM at 1.5 eV,[6,56] indicating that charge separation process is energetically favored. Nevertheless, it seems that in P3HT:PCBM blends energy transfer from P3HT to PCBM is efficient enough to form singlet the excited state of PCBM, which yields $^3PCBM*$ *via* intersystem crossing that reacts with $^3O_2$.

The drop in the absorbance of DPBF after 25 min and the corresponding quantum yields of singlet oxygen photogeneration are significantly lower for both P3HT:SWCNT and P3HT:C$_{60}$ (Fig. 3B and Table 1), which is probably related to the low solubility of C$_{60}$ and SWCNT and the thus higher tendency of the two to form agglomerates and clusters during deposition process.[57–59] It has already been shown that the lifetime of the triplet-excited state of the photosensitizer, and consequently the $^1O_2$ photogeneration efficiency, can be significantly reduced due to agglomeration. Moreover, it has been shown that carbon nanotubes can also effectively quench $^1O_2$, thus lowering its overall production yield.[60]
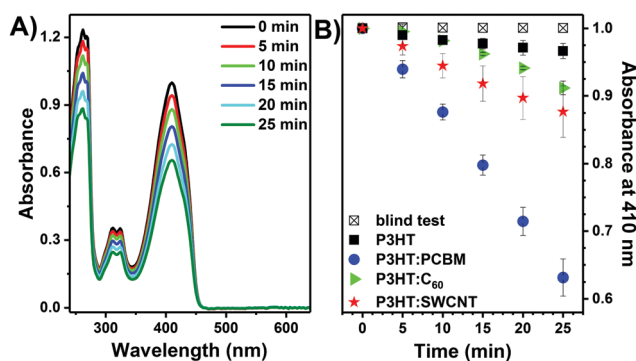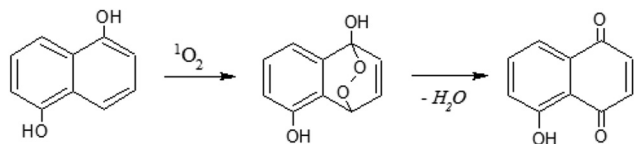

Fig. 3 (A) Representative set of UV-vis spectra of DPBF in methanol recorded during illumination of P3HT : PCBM (2 : 1) layer with a 532 nm laser. (B) Absorbance of DPBF at 410 nm as a function of time during illumination of P3HT, P3HT : PCBM (2 : 1), P3HT : C$_{60}$ (2 : 1), P3HT : SWCNT (2 : 1) deposited on borosilicate glass and bare borosilicate glass (blind test) with a 532 nm laser.

Table 1 Quantum yields of singlet oxygen photogeneration determined with the DPBF-method and Rose Bengal as reference

Photoactive layer	Φ_{CH_3OH} [%]
P3HT : C$_{60}$ (2 : 1)	< 0.5
P3HT : SWCNT (2 : 1)	< 0.5
P3HT : PCBM (2 : 1)	1.1
P3HT : PCBM (1 : 1)	2.0
P3HT : PCBM (1 : 2)	4.2
Pristine PCBM	1.9

Scheme 1 Scheme of DHN reaction with $^1O_2$ to produce juglone.

Table 2 Rate constants of DHN oxidation with singlet oxygen, photo-generated by P3HT:PCBM layers

Photoactive layer	$k \times 10^7$ (mol dm^{-3} min^{-1})
P3HT : PCBM (2 : 1)	0.90
P3HT : PCBM (1 : 1)	1.20
P3HT : PCBM (1 : 2)	3.25
Pristine PCBM	1.07

Taking the above into account, the P3HT:PCBM composite was further investigated as a heterogeneous source of singlet oxygen. Since PCBM possesses significantly higher solubility than unmodified C_{60}, it is possible to increase its concentration in the polymeric matrix, while avoiding its aggregation.

3.3. Photooxidation of 1,5-dihydroxynaphthalene

1,5-Dihydroxynaphthalene (DHN) is a commonly used substrate in fine chemical reactions in the production of juglone (5-hydroxy-1,4-naphthoquinone) an anthelmintic drug (Scheme 1), which naturally occurs in plants, especially in black walnut.[61,62] Oxidation of DHN to juglone was used as a proof of concept for singlet oxygen generation by direct measurement of the formed species. The progress of DHN oxidation can be easily monitored by UV-vis spectroscopy as changes in absorbance at 298 and 406 nm.[63,64]

The DHN photooxidation was conducted *in situ* applying photoexcitation of P3HT:PCBM layers to generate singlet oxygen. A xenon lamp was used for illumination, to excite the P3HT:PCBM films. Fig. 5A presents a set of UV-vis spectra of a DHN solution collected during illumination of the P3HT : PCBM (1 : 2) layer. The absorbance of DHN at 298 nm decreases with time, indicating its reaction with $^1O_2$ to produce juglone, also indicated by the appearance of the specific absorption band with a maximum at *ca.* 406 nm that is gradually increasing as the reaction proceeds. Almost no decrease in DHN concentration is observed when the bare glass is illuminated (Fig. 5A inset). As in the case of the DPBF test, the dissolution of the layer in the reaction mixture can be excluded, since neither

characteristic absorption bands of PCBM nor P3HT have been recorded.

Similar sets of UV-vis spectra were collected for P3HT : PCBM layers with 1 : 1 and 2 : 1 ratio. The rate constants of DHN oxidation by singlet oxygen, which is pseudo-zero order reaction under applied conditions, are given in Table 2. As mentioned, during illumination of the photoactive layers with a xenon lamp also the PCBM photosensitizer is excited directly. As expected, an increase in PCBM content increases the value of rate constant of DHN oxidation. The relation is not linear and the trend corresponds to the quantum yield of $^1O_2$ generation (Table 1). The rate constant for DHN oxidation with pristine PCBM layer is about 3-times lower than for P3HT : PCBM (1 : 2), suggesting that P3HT absorbing in the visible region plays an additional role in the formation of singlet oxygen, either directly or indirectly by energy transfer to form C_{60} triplet excited state.

In a final step, DHN photooxidation was conducted in a self-constructed photoreactor equipped with a xenon lamp as illumination source using P3HT : PCBM (1 : 2) covered glass slides with a total active area of 81 cm^2. The reaction was carried out for 4 h and samples were taken every 15 min. and analyzed by UV-vis spectroscopy. Fig. 5B shows the increase in the concentration of juglone in the reaction mixture, calculated based on the absorbance at 406 nm. The structure of the reaction product juglone was further confirmed by ^{1}H-NMR spectroscopy (ESI†). The steady increase in the absorbance of juglone with time, confirms that P3HT:PCBM photoactive layers retain activity under prolonged illumination, and thus can be effectively applied as a heterogeneous source of singlet oxygen.
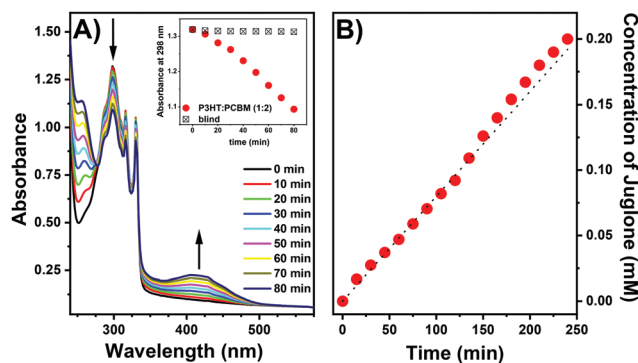
4. Conclusions

Photoactive layers based on a P3HT matrix containing carbon nanostructures as photosensitizers were investigated as photosensitizers to produce singlet oxygen. In these blends P3HT acts as a visible-light absorber and transfers energy to the carbon nanostructure, which is the actual photosensitizer that produces singlet oxygen. Singlet oxygen formation was monitored spectroscopically *in situ via* the oxidation of DPBF in methanol and was used synthetically to form juglone from DHN in acetonitrile. The efficiency of $^1O_2$ production depends on the photosensitizer and is significantly lower for blends of P3HT with C_{60} and single-walled carbon nanotubes than for blends of P3HT with PCBM. For P3HT:PCBM-based thin films, the quantum efficiency of $^1O_2$ photogeneration can be tuned by varying

Fig. 5 (A) A representative set of UV-vis spectra of DHN in acetonitrile recorded during *in situ* illumination of P3HT : PCBM (1 : 2) layer with a xenon lamp. The inset shows the decrease in absorbance at 298 nm in time. (B) Change in the juglone concentration *vs.* time in the photoreactor reaction mixture during illumination of P3HT : PCBM (1 : 2) layer with a xenon lamp.

the PCBM concentration in the P3HT layer. The results show that such easily-fabricated fullerene–polymer blends can be considered for singlet oxygen generation using visible-light and applied for fine chemicals synthesis.

Conflicts of interest

There are no conflicts to declare.

References

1 S. Ren, M. Bernardi, R. R. Lunt, V. Bulovic, J. C. Grossman and S. Gradecak, *Nano Lett.*, 2011, **11**, 5316–5321.

2 V. C. Tung, J.-H. Huang, J. Kin, A. J. Smith, C.-W. Chu and J. Huang, *Energy Environ. Sci.*, 2012, **5**, 7810–7818.

3 R. M. Williams, H. Chen, D. Di Nuzzo, S. C. J. Meskers and R. A. J. Janssen, *J. Spectrosc.*, 2017, **2017**, 6867507.

4 A. J. Gillett, A. Privitera, R. Dilmurat, A. Karki, D. Qian, A. Pershin, G. Londi, W. K. Myers, J. Lee, J. Yuan, S. J. Ko, M. K. Riede, F. Gao, G. C. Bazan, A. Rao, T. Q. Nguyen, D. Beljonne and R. H. Friend, *Nature*, 2021, **597**, 666–671.

5 J. J. Benson-Smith, H. Ohkita, S. Cook, J. R. Durrant, D. D. C. Bradley and J. Nelson, *Dalton Trans.*, 2009, 10000–10005.

6 D. Di Nuzzo, A. Aguirre, M. Shahid, V. S. Gevaerts, S. C. J. Meskers and R. A. J. Janssen, *Adv. Mater.*, 2010, **22**, 4321–4324.

7 S. Cook, H. Ohkita, J. R. Durrant, Y. Kim, J. J. Benson-smith, J. Nelson and D. D. C. Bradley, *Appl. Phys. Lett.*, 2006, **89**, 101128.

8 A. Distler, P. Kutka, T. Sauermann, H.-J. Egelhaaf, D. M. Guldi, D. Di Nuzzo, S. C. J. Meskers and R. A. J. Janssen, *Chem. Mater.*, 2012, **24**, 4397–4405.

9 M. C. DeRosa and R. J. Crutchley, *Coord. Chem. Rev.*, 2002, **233–234**, 351–371.

10 J. Wahlen, D. E. De Vos, P. A. Jacobs and P. L. Alsters, *Adv. Synth. Catal.*, 2004, **346**, 152–164.

11 I. Pibiri, S. Buscemi, A. Palumbo Piccionello and A. Pace, *ChemPhotoChem*, 2018, **2**, 535–547.

12 A. A. Ghogare and A. Greer, *Chem. Rev.*, 2016, **116**, 9994–10034.

13 P. R. Ogilby, *Chem. Soc. Rev.*, 2010, **39**, 3181–3209.

14 P. Dallas, G. Rogers, B. Reid, R. A. Taylor, H. Shinohara, G. A. D. Briggs and K. Porfyrakis, *Chem. Phys.*, 2016, **465–466**, 28–39.

15 Q. Li, H. Guo, X. Yang, S. Zhang and H. Zhang, *Tetrahedron*, 2017, **73**, 6632–6636.

16 S. Guo, H. Zhang, L. Huang, Z. Guo, G. Xiong and J. Zhao, *Chem. Commun.*, 2013, **49**, 8689–8691.

17 L. Huang, X. Cui, B. Therrien and J. Zhao, *Chem. – Eur. J.*, 2013, **19**, 17472–17482.

18 A. Blacha-Grzechnik, M. Krzywiecki, R. Motyka and M. Czichy, *J. Phys. Chem. C*, 2019, **123**, 25915–25924.

19 E. Reynoso, A. M. Durantini, C. A. Solis, L. P. Macor, L. A. Otero, M. A. Gervaldo, E. N. Durantini and D. A. Heredia, *RSC Adv.*, 2021, **11**, 23519–23532.

20 M. Bregnhøj, M. Prete, V. Turkovic, A. U. Petersen, M. B. Nielsen, M. Madsen and P. R. Ogilby, *Methods Appl. Fluoresc.*, 2020, **8**, 014001.

21 M. Wainwright, *Photodiagn. Photodyn. Ther.*, 2009, **6**, 167–169.

22 N. E. Grammatikova, L. George, Z. Ahmed, N. R. Candeias, N. A. Durands and A. Efimov, *J. Mater. Chem. B*, 2019, **7**, 4379–4384.

23 S. Noimark, C. W. Dunnill and I. P. Parkin, *Adv. Drug Delivery Rev.*, 2013, **65**, 570–580.

24 V. Decraene, J. Pratten and M. Wilson, *Appl. Environ. Microbiol.*, 2006, **72**, 4436–4439.

25 C. Piccirillo, S. Perni, J. Gil-Thomas, P. Prokopovich, M. Wilson, J. Pratten and I. P. Parkin, *J. Mater. Chem.*, 2009, **19**, 6167–6171.

26 G. B. Hwang, E. Allan and I. P. Parkin, *ACS Appl. Mater. Interfaces*, 2016, **8**, 15033–15039.

27 M. Krouit, R. Granet and P. Krausz, *Eur. Polym. J.*, 2009, **45**, 1250–1259.

28 C. Ringot, V. Sol, M. Barrière, N. Saad, P. Bressollier, R. Granet, P. Couleaud, C. Frochot and P. Krausz, *Biomacromolecules*, 2011, **12**, 1716–1723.

29 E. A. Lukina, I. P. Pozdnyakov, A. S. Mereshchenko, M. N. Uvarov and L. V. Kulik, *J. Photochem. Photobiol., A*, 2015, **311**, 193–198.

30 R. A. J. Janssen, N. S. Sariciftci and A. J. Heeger, *J. Chem. Phys.*, 1994, **100**, 8641–8645.

31 A. J. Ferguson, J. L. Blackburn, J. M. Holt, N. Kopidakis, R. C. Tenent, T. M. Barnes, M. J. Heben and G. Rumbles, *J. Phys. Chem. Lett.*, 2010, **1**, 2406–2411.

32 A. R. S. Kandada, G. Grancini, A. Petrozza, S. Perissinotto, D. Fazzi, S. S. K. Raavi and G. Lanzani, *Sci. Rep.*, 2013, **3**, 2073.

33 G. Beamson and D. Briggs, *XPS of Organic Polymers*, John Wiley & Sons, Chichester, 1992.

34 M. Wainwright, *Dyes Pigm.*, 2007, **73**, 7–12.

35 K. Piwowar, A. Blacha-Grzechnik, R. Turczyn and J. Zak, *Electrochim. Acta*, 2014, **141**, 182–188.

36 F. Lv, Y. Yu, E. Hao, C. Yu, H. Wang and L. Jiao, *Org. Biomol. Chem.*, 2019, **17**, 1–44.

37 C. R. Lambert and I. E. Kochevar, *J. Am. Chem. Soc.*, 1996, **118**, 3297–3298.

38 M. I. Burguete, F. Galindo, R. Gavara, S. V. Luis, M. Moreno and D. A. Russell, *Photochem. Photobiol. Sci.*, 2009, **8**, 37–44.

39 N. Epelde-Elezcano, V. Martinez-Martinez, E. Pena-Cabrera, C. F. A. Gomez-Duran, I. L. Arbeloa and S. Lacombe, *RSC Adv.*, 2016, **6**, 41991–41998.

40 R. A. Marsh, J. M. Hodgkiss, S. Albert-Seifried and R. H. Friend, *Nano Lett.*, 2010, **10**, 923–930.

41 U. Zhokhavets, T. Erb, G. Gobsch, M. Al-Ibrahim and O. Ambacher, *Chem. Phys. Lett.*, 2006, **418**, 347–350.

42 B. Kadem, A. Hassan and W. Cranton, *J. Mater. Sci.: Mater. Electron.*, 2016, **27**, 7038–7048.

43 F. Otieno, B. K. Mutuma, M. Airo, K. Ranganathan and R. Erasmus, *Thin Solid Films*, 2017, **625**, 62–69.

44 Y.-C. Huang, Y.-C. Liao, S.-S. Li, M.-C. Wu, C.-W. Chen and W.-F. Su, *Sol. Energy Mater. Sol. Cells*, 2009, **93**, 888–892.

45 B. Y. Kadem, M. K. Al-hashimi and A. K. Hassan, *Energy Procedia*, 2014, **50**, 237–245.

46 Y. Yang, S. Feng, M. Li, Z. Wu, X. Fang, F. Wang, D. Geng, T. Yang, X. Li, B. Sun and X. Gao, *ACS Appl. Mater. Interfaces*, 2015, **7**, 24430–24437.

47 R. V. Bensasson, E. Bienvenue, M. Dellinger, S. Leach and P. Seta, *J. Phys. Chem.*, 1994, **98**, 3492–3500.

48 P. J. Goutam, D. K. Singh and P. K. Iyer, *J. Phys. Chem. C*, 2012, **116**, 8196–8201.

49 J. U. Lee, A. Cirpan, T. Emrick, T. P. Russell and W. H. Jo, *J. Mater. Chem.*, 2009, **19**, 1483–1489.

50 H. Chadli, A. Rahmani and J.-L. Sauvajol, *J. Phys.: Condens. Matter*, 2010, **22**, 145303.

51 C.-Y. Su, A.-Y. Lu, Y.-L. Chen, C.-Y. Wei, P.-C. Wang and C.-H. Tsai, *J. Mater. Chem.*, 2010, **20**, 7034–7042.

52 A. P. P. Alves, J. P. C. Trigueiro, H. D. R. Calado and G. G. Silva, *Electrochim. Acta*, 2011, **209**, 111–120.

53 G. J. H. Melvin, Q.-Q. Ni, Y. Suzuki and T. Natsuki, *J. Mater. Sci.*, 2014, **49**, 5199–5207.

54 W. Li, L. Li, H. Xiao, R. Qi, Y. Huang, Z. Xie, X. Jing and H. Zhang, *RSC Adv.*, 2013, **3**, 13417–13421.

55 M. Narutaki, K. Takimiya, T. Otsubo, Y. Harima, H. Zhang, Y. Arki and O. Ito, *J. Org. Chem.*, 2006, **71**, 1761–1768.

56 K. Vandewal, K. Tvingstedt, A. Gadisa, O. Inganäs and J. V. Manca, *Phys. Rev. B: Condens. Matter Mater. Phys.*, 2010, **81**, 125204.

57 S. Wang, R. Gao, F. Zhou and M. Selke, *J. Mater. Chem.*, 2004, 487–493.

58 R. S. Ruoff, D. S. Tse, R. Malhotra and D. C. Lorents, *J. Phys. Chem.*, 1993, **97**, 3379–3383.

59 S. Berson, R. De Bettignies, S. Bailly, S. Guillerez and B. Jousselme, *Adv. Funct. Mater.*, 2007, **17**, 3363–3370.

60 N. Gandra, P. L. Chiu, W. Li, Y. R. Anderson, S. Mitra, H. He and R. Gao, *J. Phys. Chem. C*, 2009, **113**, 5182–5185.

61 S. Cosmulescu, I. Trandafir, G. Achim and A. Baciu, *Not. Bot. Horti Agrobot. Cluj-Napoca*, 2011, **39**, 237–240.

62 S. Sugie, K. Okamoto, K. M. W. Rahman, T. Tanaka, K. Kawai, J. Yamahara and H. Mori, *Cancer Lett.*, 1998, **127**, 177–183.

63 S. Takizawa, R. Aboshi and S. Murata, *Photochem. Photobiol. Sci.*, 2011, **10**, 895–903.

64 M. Luiz, A. T. Soltermann, A. Biasutti and N. A. Garcia, *Can. J. Chem.*, 2006, **74**, 49–54.